analytical chemistry

pubs.acs.org/ac Article

A Host–Guest Interaction-Based and Metal–Organic Gel-Based Biosensor with Aggregation-Induced Electrochemiluminescence Enhancement for Methyltransferase Assay

Lin Cui,† Min-hui Zhao,† Chen-chen Li,† Quanbo Wang, Xiliang Luo,* and Chun-yang Zhang*

Cite This: *Anal. Chem.* 2021, 93, 2974–2981 Read Online

ACCESS | Metrics & More | Article Recommendations | Supporting Information

ABSTRACT: Metal–organic gels (MOGs) are new soft materials with the characteristics of high colloidal stability, superb luminescence properties, and facile synthesis. Herein, we develop for the first time a host–guest interaction-based and MOG-based biosensor with aggregation-induced electrochemiluminescence (ECL) enhancement for M.SssI methyltransferase (M.SssI MTase) assay. This biosensor employs a MOG as the luminophor and potassium persulfate as the coreactant, and the formation of the Ag-MOG from the aggregation of silver nanoclusters can induce significant ECL enhancement. Two complementary single-stranded DNAs (ssDNAs, i.e., biotinylated DNA-1 and Fc-labeled DNA-2) that contain specific recognition sequence 5′-CCGG-3′ can form a double-stranded DNA (dsDNA) probe. In the absence of M.SssI MTase, the dsDNA probe will be digested by restriction endonuclease HpaII, leading to the release of Fc from magnetic beads (MBs). The β-CD can specifically recognize the released Fc through guest–host interaction, resulting in the quenching of an ECL signal. In contrast, the presence of M.SssI MTase enables the formation of fully methylated dsDNA, which cannot be cleaved by HpaII, making Fc remain on the MB surface and consequently generating an improved ECL signal. This biosensor can specifically detect M.SssI MTase with a linear range of 0.05–100 U mL^{-1} and a limit of detection of 3.5 × 10^{-3} U mL^{-1}, and it enables accurate detection of M.SssI MTase in human serum. In addition, it can be used for inhibitor screening, with wide applications in drug discovery and disease diagnosis.

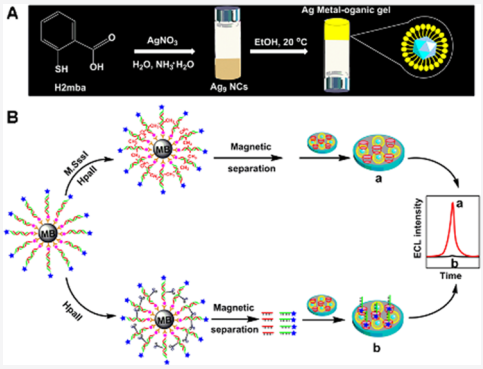

Deoxyribonucleic acid (DNA) methylation enables the transfer of a methyl group from S-adenosyl-L-methionine (SAM) to the C-5 position of cytosine in the CpG dinucleotides,[1] and it plays essential roles in genomic imprinting, gene expression, and X-chromosome inactivation.[2] Alterations of methyltransferase (MTase) activity can induce aberrant DNA methylation patterns and cause a variety of cancers and genetic diseases.[3] Consequently, DNA MTase may function as an important biomarker,[4] and different kinds of methods have been introduced for DNA MTase activity assay, including high-performance liquid chromatography,[5] real-time quantitative polymerase chain reaction,[6] gas chromatography/mass spectrometry,[7] high-performance capillary electrophoresis,[8] colorimetric assay,[9] fluorescence assay,[10,11] and chemiluminescence assay.[12,13] However, most of them involve expensive instruments and laborious sample treatment. The development of cost-effective and sensitive methods for MTase activity assays has remained a challenge.

Electrochemiluminescence (ECL) is a chemiluminescence reaction on the surface of electrodes,[14] and it can precisely control the location and time of light emission, with the characteristics of good reproducibility and high sensitivity.[15] ECL has been widely applied in bioanalysis and diagnosis.[16,17] The emitters of luminophores for ECL studies include luminol,[18,19] ruthenium(II) complexes,[20] metal clusters,[21] quantum dots,[22] and halide perovskite nanomaterials,[23] but most of them are detrimental to modification with the shortcomings of high price, weak stability, and complicated steps. The aggregation-induced emission (AIE) results from the restriction of intramolecular motions, vibrations, and rotations.[24] AIE carves out a new avenue for the development of novel biosensors[25−27] with wide applications in biomedical research.[28] The metal nanocrystal-mediated AIE has been first discovered in organic molecules that possesses a propeller-like structure.[29] Some typical AIE examples include Au,[30] Ag,[31,32] and Cu nanocrystals[33] and their hybrids.[34] The reported AIE from the coordinated metal nanocrystals was carried out in either dilute aqueous solution or organic solvent.[35] In 2017, the aggregation-induced electrochemiluminescence was reported for the first time in a pyridine-containing Pt(II) complex system.[36] The integration of AIE with ECL can

Received: November 20, 2020
Accepted: January 13, 2021
Published: January 21, 2021

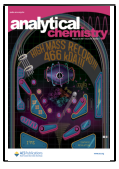

https://dx.doi.org/10.1021/acs.analchem.0c04904
Anal. Chem. 2021, 93, 2974–2981

significantly enhance an ECL signal,[36,37] opening a new avenue for the design of novel ECL-based sensors.[15,38]

Metal−organic gels (MOGs) have emerged as a new type of metal−organic hybrid material, and they can be rapidly built up by straightforward self-assembling from metal ions and organic ligands through metal−ligand interactions and intermolecular forces.[39−41] In particular, MOGs can be obtained by a facile and mild strategy (e.g., neutral condition, relatively low reaction temperature, routine solvents, and short reaction time). Due to the well-defined metal−ligand catalytically active sites, high thermal stability, large surface areas, and unique porous structures,[42] MOGs have been widely applied in the fields of adsorption,[39] catalysis,[43,44] drug delivery,[45] sensing,[46−50] white-light-emitting diodes,[51] and environmental pollution abatement.[52,53] Recently, Li's group employed the silver-based MOG as the solid coreactants to enhance the ECL of $Ru(bpy)_3^{2+}$ for DNA assay, with the MOG being used for the loading of $Ru(bpy)_3^{2+}$ molecules.[48] In addition, Li's group synthesized terbium metal−organic gels (TOGs) and employed the cathode ECL emission of TOGs for the detection of tetracycline, with TOGs being used as the luminophor.[49] However, the development of MOG-based ECL biosensors for sensitive detection of enzyme activity has remained unexplored. Herein, we develop for the first time a host−guest interaction-based and MOG-based biosensor with aggregation-induced ECL enhancement for sensitive detection of M.SssI methyltransferase (M.SssI MTase). This biosensor employs a MOG as the luminophor and potassium persulfate as the coreactant, and the formation of the Ag-MOG from the aggregation of silver nanoclusters can induce significant ECL enhancement. This biosensor can specifically detect M.SssI MTase with a linear range of 0.05−100 U mL^{-1} and a limit of detection (LOD) of 3.5×10^{-3} U mL^{-1}, and it can be used to accurately detect M.SssI MTase in human serum and screen potential inhibitors.

1. EXPERIMENTAL SECTION

1.1. Reagents and Materials. Tris(hydroxymethyl)-aminomethane (Tris), 5-azacytidine (5-Aza), $AgNO_3$, and 2-mercaptobenzoic acid (H_2mba) were obtained from Sigma-Aldrich Chemical Co. (St. Louis, MO). M.SssI CpG methyltransferase (M.SssI MTase), restriction endonuclease HpaII, Dam methyltransferase (Dam MTase), HhaI methyltransferase (HhaI MTase), and S-adenosyl-L-methionine (SAM) were bought from New England Biolabs Inc. (Beverly, MA). Streptavidin-coated magnetic beads (MBs) were obtained from New England Biolabs (NEB, UK). Ultrapure water was prepared using a Millipore water purification system (Milli-Q, Millipore). The oligonucleotides were synthesized by Sangon Biological Engineering Technology & Services Co., Ltd. (Shanghai, China). The DNA-1 sequence is 5′-CAG TCC GGA GGT G-biotin-3′, and its complementary DNA-2 sequence is 5′-CAC CTC CGG ACT G-Fc-3′, with the cutting bases being shown with underline.

1.2. Apparatus and Characterization. A MPI-EII multifunctional electrochemical and chemiluminescence analytical system (Xi'an Remex Analytical Instrument Co., Ltd., China) was used for electrochemiluminescence measurements, with the emission window laying above the photomultiplier tube biased at 800 V. Electrochemiluminescence signals were measured by using Ag/AgCl (saturated KCl), a platinum wire, and a modified glassy carbon electrode (GCE, 4 mm in diameter, Gaossunion, Wuhan, China) as the reference, counter, and working electrodes, respectively. Electrochemical impedance spectroscopy (EIS) was obtained using a Zahner workstation (Zahner, German). A JEOL JEM 2010 electron microscope (JEOL Ltd., Japan) was employed for transmission electron micrograph (TEM) imaging, a SU-8010 scanning electronic microscope (SEM, Hitachi) was used for SEM imaging, and a Rigaku D/MAX 2200PC X-ray diffractometer (X'Pert Pro Super, Philips) was used to obtain the powder X-ray diffraction (XRD) patterns. Fourier transform infrared (FT-IR) spectra were obtained using a Thermo Scientific Nicolet iS50 FT-IR spectrophotometer, and X-ray photoelectron spectroscopy (XPS) was performed using an ESCALAB 250 X-ray photoelectron spectrometer with a monochromatized Al Kα X-ray source (1486.71 eV), and the absorption spectra were obtained using a UV-3900 spectrophotometer (Hitachi, Japan).

1.3. Synthesis of the Ag-MOG. The Ag-MOG was prepared according to a previous report.[53] Briefly, H_2mba (1 mmol, 155 mg) and $AgNO_3$ (1 mmol, 170 mg) were added into 6 mL of water, followed by sonication for 20 min in a KQ5200DE instrument (Kunshan Ultrasonic Instruments Co., China). During an ultrasonic process, the addition of 0.5 mL of $NH_3{\cdot}H_2O$ (25%) leads to the formation of a yellow clear solution containing Ag_9NCs. Then, the mixture of 5.0 mM Ag_9NC and 70% ethanol was shaken gently at 20.0 ± 0.1 °C for gelation to obtain the Ag-MOG. Eventually, the Ag-MOG was dried by a freeze-drying process to obtain the Ag-MOG powder.

1.4. Preparation of MB/dsDNA Probes. The DNA-1/DNA-2 hybrids (dsDNAs) were obtained by incubating DNA-1 with DNA-2 in a hybridization buffer (1.0 mM EDTA, 1.0 M NaCl, 10 mM Tris, pH 7.4) at 37 °C for 30 min. A total of 10 μL of streptavidin-modified MBs was washed three times with 50 μL of washing buffer (1 mM EDTA, 0.5 M NaCl, 20 mM tris-HCl, pH 7.4) and resuspended in 190 μL of 1× PBS, followed by incubation with 10 μL of 10 μM dsDNA probes for 30 min to obtain the MB-linked dsDNA probes through biotin−streptavidin interaction. After washing three times with the washing buffer, the obtained MB-linked dsDNA probes were dispersed in 100 μL of 1× PBS buffer.

1.5. Fabrication of Electrochemiluminescence Platform. The GCE was polished to a mirror-like surface prior to the modification. The Ag-MOG/GCE was obtained by dropping 20 μL of 0.5 mg mL^{-1} Ag-MOG onto the working electrode at room temperature. Then, 20 μL of β-CD solution (3 mM) was sequentially dropped on the working electrode, followed by drying to obtain the β-CD/Ag-MOG/GCE.

1.6. Electrochemiluminescence Measurement of M.SssI MTase Activity and Inhibitor Assay. A total of 10 μL of MB-linked dsDNA probes was incubated with 20 μL of reaction solution, which contains 160 μM SAM, 2.0 μL of 1× NEBuffer 2, and different concentrations of M.SssI MTase at 37 °C for 2 h. Then, the supernatants were removed by magnet separation, followed by washing with the washing buffer. Subsequently, the MB-linked dsDNA probes were incubated with 1× CutSmart buffer (2.0 μL) containing 80 U mL^{-1} HpaII restriction endonuclease for 2 h at 37 °C. After magnetic separation, the supernatant was added to the electrode, followed by incubation for 50 min. The ECL measurements were performed in 10 mM $K_2S_2O_8$ + PBS solution (pH 7.4). For inhibition assay, 100 U mL^{-1} M.SssI MTase was incubated with different concentrations of inhibitors, followed by the same procedures as M.SssI MTase assay.

https://dx.doi.org/10.1021/acs.analchem.0c04904
Anal. Chem. 2021, 93, 2974−2981

2. RESULTS AND DISCUSSION

2.1. Principle of M.SssI MTase Assay. Scheme 1A shows the schematic illustration for the synthesis of the Ag-MOG.

Scheme 1. (A) Schematic Illustration for the Synthesis of the Ag Metal−Organic Gel (Ag-MOG). (B) Schematic Illustration for the Detection of M.SssI MTase Activity Using the ECL Biosensor

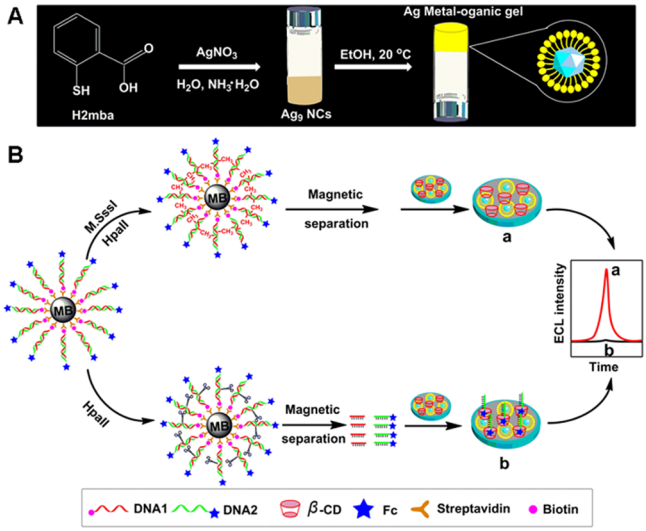

After mixing $AgNO_3$ with H_2mba at room temperature, $NH_3 \cdot H_2O$ was added into the solution to obtain the Ag_9NCs. The subsequent addition of ethanol (EtOH) may induce the decreased solubility of Ag_9NCs and the consequent gelation,[54] resulting in the formation of the Ag-MOG with high colloidal stability. Scheme 1B shows the principle of M.SssI MTase detection using the ECL biosensor. We designed two complementary ssDNA strands, with DNA-1 containing specific recognition sequence 5′-CCGG-3′ and a biotin group at the 3′ end and DNA-2 containing specific recognition sequence 5′-CCGG-3′ and an Fc label at the 3′ end. DNA-1 is assembled on the streptavidin-coated magnetic beads (MBs) through specific streptavidin−biotin interaction and subsequently hybridizes with DNA-2 to form the dsDNA probe, which contains the specific recognition sequence (i.e., 5′-CCGG-3′) of both M.SssI MTase and HpaII. In the absence of target M.SssI MTase, the CpG dinucleotide site of 5′-CCGG-3′ cannot be methylated, resulting in the digestion of dsDNA probes by HpaII. After magnetic separation, the β-CD can recognize the released Fc from the MB through guest−host interaction, leading to the quenching of ECL emission by Fc. When M.SssI MTase is present, it catalyzes the methylation of CpG dinucleotides in dsDNA probes, and the methylated dsDNA probes cannot be digested by HpaII endonuclease, leading to the remaining of dsDNA probes on the MB surface. As a result, no free Fc is available in the supernatant for the quenching of an ECL signal, and an enhanced ECL signal can be observed.

2.2. Characteristics of the Ag-MOG. The crystal structure of the Ag-MOG is characterized by an XRD pattern (Figure 1A). A series of sharp peaks within a wide 2θ range from 2 to 40° are observed, indicating the amorphous nature of the obtained Ag-MOG.[52] The SEM (Figure 1B) and TEM (Figure 1C) of the Ag-MOG indicate the entangled fibers in the gel. The FT-IR spectrometer was used to verify the

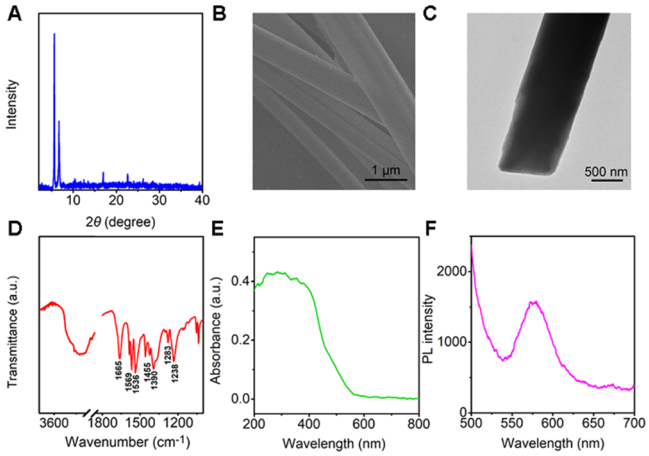

Figure 1. (A) XRD pattern, (B) SEM image, and (C) TEM image of the Ag-MOG. (D) FT-IR spectrum, (E) diffuse reflectance spectrum, and (F) photoluminescence spectrum of the Ag-MOG. The excitation wavelength is 234 nm.

multiple inter- and intracluster interactions (especially the hydrogen bond). As shown in Figure 1D, after gelation, the asymmetric stretching of C═O blue shifts from 1680 to 1665 cm^{-1} and the peak of −OH at 3200 cm^{-1} becomes broader. The symmetric stretching of C═O at 1377 cm^{-1} disappears, and some new peaks emerge in a range of 1570−1235 cm^{-1}. These changes can be ascribed to the formation of hydrogen bonds including the O−H···O bonds between the adjacent Ag_9NCs or between Ag_9 and the solvent molecule as well as the N−H···O bonds between NH_4^+ and Ag_9NCs. The UV−vis diffuse reflectance spectrum (DRS) can characterize the electronic transitions of different orbitals of a solid and the band gap energy (E_g) of polymers. The DRS of the Ag-MOG exhibits broad absorption range in the visible region (Figure 1E). The band gap of the Ag-MOG can be obtained from the absorption edges according to eq 1

$$E_g\ (\mathrm{eV}) = hc/\lambda \tag{1}$$

The band gap of the Ag-MOG is calculated to be 2.48 eV. We further measured the photoluminescence (PL) spectrum of the Ag-MOG (Figure 1F). An emission peak at 575 nm is obtained at an excitation wavelength of 234 nm.

2.3. Study of the ECL Mechanism. The ECL mechanism of the Ag-MOG/$S_2O_8^{2-}$ system is proposed in Scheme 2. In

Scheme 2. ECL Mechanism of the Ag-MOG−$S_2O_8^{2-}$ System

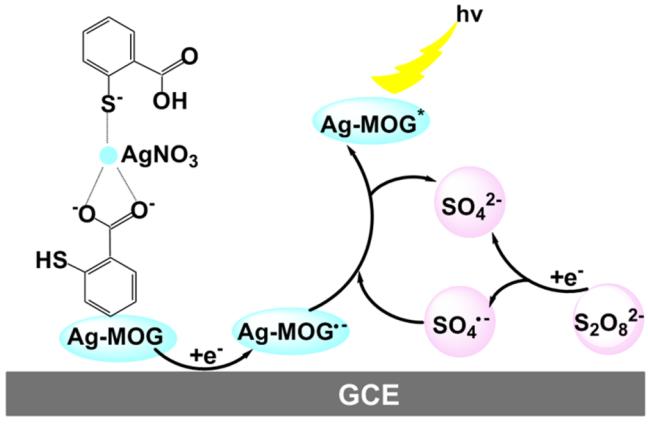

https://dx.doi.org/10.1021/acs.analchem.0c04904
Anal. Chem. 2021, 93, 2974−2981

the canodic scanning process, the Ag-MOG is oxidized to form an anion radical Ag-MOG$^{\cdot-}$ (eq 2). Meanwhile, the electroreduction of coreactant $S_2O_8^{2-}$ produces a $S_2O_8^{2\cdot-}$ anion radical (eq 3). Subsequently, a $S_2O_8^{2\cdot-}$ cation radical generates a strong oxidant $SO_4^{\cdot-}$ (eq 4). The $SO_4^{\cdot-}$ radical can inject a hole into the Ag-MOG$^{\cdot-}$, producing an excited-state Ag-MOG* (eq 5). When Ag-MOG* decays back to the ground state, a distinct emission is generated (eq 6). To verify the ECL mechanism of the Ag-MOG, we measured the ECL signals and cyclic voltammetry (CV) of the GCE and the Ag-MOG-modified GCE, respectively (Figure 2). Notably, no ECL signal

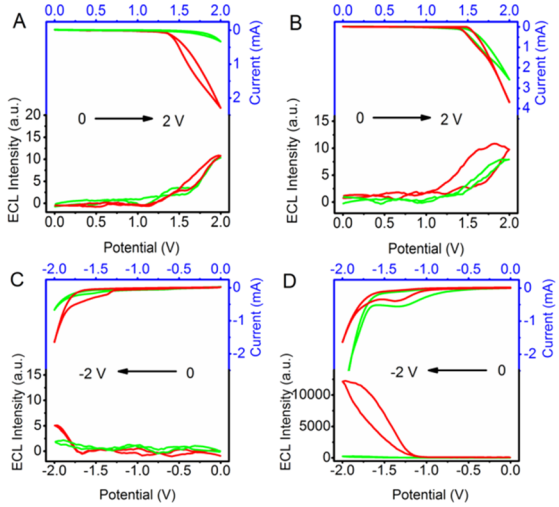

Figure 2. ECL−potential profiles (bottom) and the corresponding CV curves (top) of the bare GCE (green) and the Ag-MOG/GCE (red) in scanning ranges of (A) 0−2 V and (C) 0 to −2 V in 0.1 M PBS. ECL−potential profiles (bottom) and CV curves (top) of the Ag-MOG/GCE (red) and bare GCE (green) (B) in a scanning range of 0−2 V in 10 mM TPrA + 0.1 M PBS and (D) in a scanning range of 0 to −2 V in 10 mM $S_2O_8^{2-}$ + 0.1 M PBS (D).

is observed for both the bare GCE (Figure 2A,B, green) and the Ag-MOG/GCE (Figure 2A,B, red) in either PBS or PBS + TPrA in a potential range of 0−2 V, suggesting that the ECL of the Ag-MOG does not undergo an anode coreactant pathway. Figure 2C shows the ECL signals and CVs of the bare GCE (Figure 2C, green) and the Ag-MOG-modified GCE (Figure 2C, red) in a potential range of 0 to −2 V in 0.1 M PBS (pH 7.4). The bare GCE shows neither apparent redox peaks (Figure 2C, top green) nor an ECL signal (Figure 2C, bottom green) in PBS. However, the CV curve of the Ag-MOG-modified GCE (Figure 2C, top red) in PBS exhibits a reduction peak at −1.35 V with no ECL signal being observed, suggesting that the Ag-MOG undergoes a weak reduction process (Figure 2C, bottom red). In the presence of $S_2O_8^{2-}$ (Figure 2D), $S_2O_8^{2-}$ undergoes a reduction process at −1.26 V to produce a $S_2O_8^{2\cdot-}$ anion radical in the bare GCE (Figure 2D, top green), generating a low ECL signal (200 a.u.). The onset of ECL for the Ag-MOG in the presence of $S_2O_8^{2-}$ is at −1.1 V, at which anion radical Ag-MOG$^{\cdot-}$ is generated (Figure 2D, bottom red). The reduction peak of the CV curve of the Ag-MOG-modified GCE (Figure 2D, top red) in the presence of $S_2O_8^{2-}$ is located at −1.34 V, close to the peak potential of the Ag-MOG in PBS (Figure 2C, top red), suggesting that they undergo the same reduction process to produce the Ag-MOG$^{\cdot-}$. When scanning to more negative potentials, the ECL signal of the Ag-MOG-modified GCE becomes higher and higher with an ECL maximum being observed at −1.7 V (Figure 2D, bottom red), indicating the generation of more radical species Ag-MOG$^{\cdot-}$. Notably, the ECL intensity of the Ag-MOG in $S_2O_8^{2-}$ (12,000 a.u.) is 60- and 2000-fold higher than that of bare GCE in $S_2O_8^{2-}$ (200 a.u., Figure 2D, bottom green) and the Ag-MOG without $S_2O_8^{2-}$ (6 a.u., Figure 2C, bottom red), respectively, further confirming the ECL mechanism of the Ag-MOG/$S_2O_8^{2-}$ system (Scheme 2). We further investigated the ECL of Ag_9NCs and H_2mba in either PBS or $S_2O_8^{2\cdot-}$, respectively (Figure S2, Supporting Information). Even in the presence of $S_2O_8^{2-}$, the ECL signal of either the Ag_9NC-modified (2200 a.u.) or H_2mba-modified (380 a.u.) GCE is smaller than that of the Ag-MOG-modified GCE (12,000 a.u.), suggesting the aggregation-induced ECL, which results from the formation of the Ag-MOG via the reaction of Ag_9NCs with H_2mba.

$$\text{Ag} - \text{MOG} + e^- \rightarrow \text{Ag} - \text{MOG}^{\cdot-} \quad (2)$$

$$S_2O_8^{2-} + e^- \rightarrow S_2O_8^{2\cdot-} \quad (3)$$

$$S_2O_8^{2\cdot-} \rightarrow SO_4^{2-} + SO_4^{\cdot-} \quad (4)$$

$$\text{Ag} - \text{MOG}^{\cdot-} + SO_4^{\cdot-} \rightarrow \text{Ag} - \text{MOG}^{*} + SO_4^{2-} \quad (5)$$

$$\text{Ag} - \text{MOG}^{*} \rightarrow \text{Ag} - \text{MOG} + h\nu \quad (6)$$

Although the ECL intensities of H_2mba (Figure 3A) and Ag_9NCs (Figure 3B) can reach 380 and 2200 a.u., respectively,

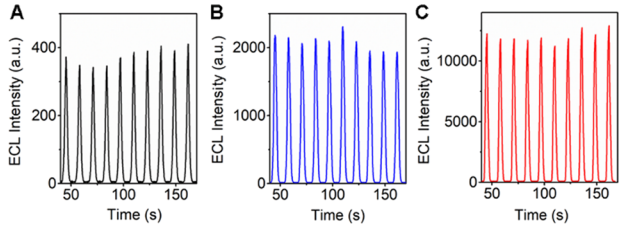

Figure 3. ECL response curves of the different electrodes modified with (A) H_2mba, (B) Ag_9NCs, and (C) Ag-MOG in 10 mM $S_2O_8^{2-}$ + 0.1 M PBS.

the signal is not very stable (Figure 3A), which is not suitable for practical applications. In contrast, the Ag-MOG can generate a very strong and stable ECL signal (12,000 a.u., Figure 3C). The canodic ECL emission of the Ag-MOG-modified GCE (Figure 3C) occurs at −1.35 V, and the ECL intensity of the Ag-MOG-modified GCE measured in 10 mM $S_2O_8^{2-}$ + 0.1 M PBS is 32- and 5.5-fold higher than that of the H_2mba-modified (Figure 3A) and Ag_9NC-modified (Figure 3B) GCE, respectively. Notably, the ECL intensity of the Ag-MOG-modified GCE (Figure 3C) is higher than that of the Ag_9NC-modified GCE (Figure 3B), suggesting the aggregation-induced ECL enhancement. This result is consistent with the previous report that the self-assembly of Ag_9NCs into the highly ordered fibers induces enhanced photoluminescence.[54] The relative standard deviation (RSD) values of the GCE modified with H_2mba, Ag_9NCs, and Ag-MOG are 6.18%, 5.55%, and 3.97%, respectively, indicating the good stability of the Ag-MOG-modified GCE.

2.4. Assay Feasibility. The interfacial study was carried out by using electrochemical impedance spectra (EIS). Figure 4A shows the EIS of the modified electrodes in different

https://dx.doi.org/10.1021/acs.analchem.0c04904
Anal. Chem. 2021, 93, 2974−2981

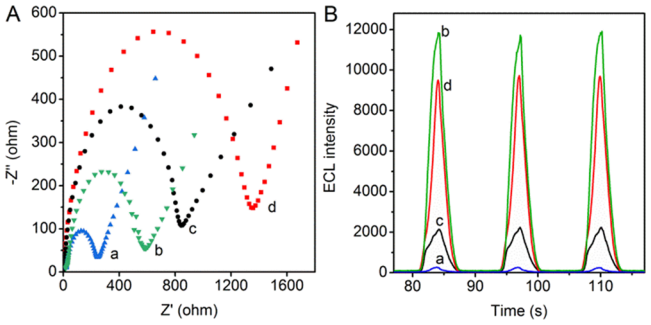

Figure 4. (A) Nyquist plots of the different modified electrodes: (a) GCE, (b) Ag-MOG/GCE, (c) β-CD/Ag-MOG/GCE, and (d) β-CD/Ag-MOG/GCE treated with the released Fc from MBs. The 100 U mL^{-1} M.SssI MTase and 80 U mL^{-1} HpaII were used in the experiments. (B) ECL intensity of the GCE (a, blue color), the Ag-MOG/GCE (b, green color), and the β-CD/Ag-MOG/GCE in response to the MB/dsDNA probes + 80 U mL^{-1} HpaII in the presence (d, red color) and absence (c, black color) of M.SssI MTase. The concentration of M.SssI MTase is100 U mL^{-1}.

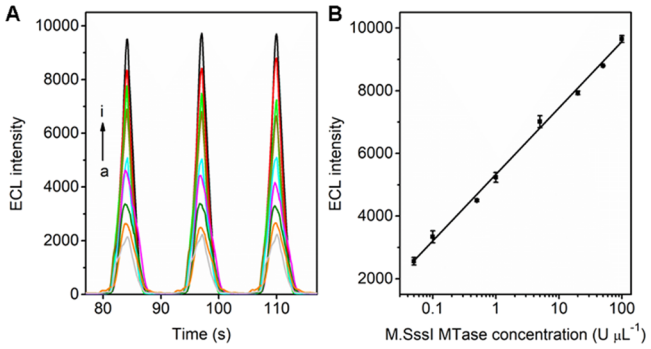

Figure 5. (A) ECL intensity generated by different concentrations of M.SssI MTase in PBS + 10 mM $K_2S_2O_8$. (B) ECL intensity exhibits a linear relationship with the logarithm of M.SssI MTase concentration. Error bars represent the standard deviations of three experiments.

construction steps. The bare GCE displays a small semicircle diameter and a long tail with a charge-transfer resistance (R_{ct}) of 250 Ω, indicating the diffusion of $Fe(CN)_6^{3-/4-}$ to the electrode surface (Figure 4A, curve a). Upon the coating of the Ag-MOG onto the GCE, the R_{ct} increases from 250 Ω (for the bare GCE, Figure 4A, curve a) to 586 Ω (Figure 4A, curve b) because the Ag-MOG possesses poor conductivity. When the β-CD is assembled onto the Ag-MOG/GCE, the R_{ct} further increases to 851 Ω (Figure 4, curve c) due to the introduction of nonconductive β-CD. A further increase in R_{ct} to 1352 Ω is observed (Figure 4A, curve d) when MB-linked dsDNA probes react with 100 U mL^{-1} M.SssI MTase and 100 U mL^{-1} HpaII.

We further investigated the biosensor with different modified surfaces (Figure 4B). A higher ECL signal is detected on the Ag-MOG-modified GCE in 10 mM $K_2S_2O_8$ + PBS (pH 7.4) solution (12,000 a.u., Figure 4B, curve b) than on the bare GCE (200 a.u., Figure 4B, curve a), indicating that the Ag-MOG can function as an excellent ECL luminophor. Notably, the ECL intensity in response to M.SssI MTase (9670 a.u., Figure 4B, curve d) is higher than that without M.SssI MTase (2200 a.u., Figure 4B, curve c), suggesting that this ECL biosensor can be applied to detect M.SssI MTase.

2.5. Sensitivity of M.SssI MTase Assay. Under the optimized experimental conditions (Figure S3), the ECL biosensor was used to measure different concentrations of M.SssI MTase in 10 mM $K_2S_2O_8$ + 0.1 M PBS (pH 7.4) solution. As shown in Figure 5A, the ECL intensity improves with the increasing concentration of M.SssI MTase. In the logarithm scale, the ECL intensity shows a linear correlation with the concentration of M.SssI MTase in a range of 0.05−100 U mL^{-1} (Figure 5B). The regression equation is I_{ECL} = 5328 + 2119 $\log_{10}C$ (R^2 = 0.9959), where I_{ECL} represents the ECL intensity and C represents the concentration of M.SssI MTase (U mL^{-1}). A LOD of 3.5 × 10^{-3} U mL^{-1} is obtained based on the control group plus three times standard deviation. The sensitivity of the proposed ECL biosensor is much higher than those of the reported methods[55−64] (Table S1), with 7.1-fold higher than that of electrochemical assay,[56−60] 8.6-fold higher than that of electrochemiluminescence assay,[55] 10-fold higher than that of photoelectrochemical assay,[61] 40-fold higher than that of fluorescence assay,[62,63] and 714.3-fold higher than that of colorimetric assay.[64] The high sensitivity of this biosensor can be ascribed to (1) the strong ECL emission of the Ag-MOG induced by target M.SssI MTase, (2) the high quenching efficiency of Fc in the absence of target M.SssI MTase, and (3) the efficient supramolecular host−guest recognition reaction.

2.6. M.SssI MTase Inhibition Assay. For inhibition assay, we used 5-aza-2′-deoxycytidine (5-Aza-dC) and 5-azacytidine (5-Aza) as the model inhibitors. The inhibition effect can be calculated based on eq 7

$$\mathrm{RA}(\%) = \frac{N_i - N_0}{N_t - N_0} \times 100\% \quad (7)$$

where N_0, N_t, and N_i represent the ECL intensity without M.SssI MTase, in the presence of 100 U mL^{-1} M.SssI MTase, and in the presence of 100 U mL^{-1} M.SssI MTase + different concentrations of 5-Aza (or 5-Aza-dC), respectively. We measured the half-maximal inhibitory concentration (IC_{50}) of 5-Aza (Figure 6A) and 5-Aza-dC (Figure 6B). The relative activity of M.SssI MTase decreases with the increasing concentration of 5-Aza in a dose-dependent manner (Figure 6A). The measured IC_{50} value (1.36 μM) is consistent with that obtained by the electrochemical assay (2.4 μM).[52] Moreover, the relative activity of M.SssI MTase decreases with the increasing concentration of 5-Aza-dC in a dose-dependent manner (Figure 6B). The measured IC_{50} value (0.69 μM) is consistent with that obtained by using a glucometer as the signal transducer (0.67 μM).[65]

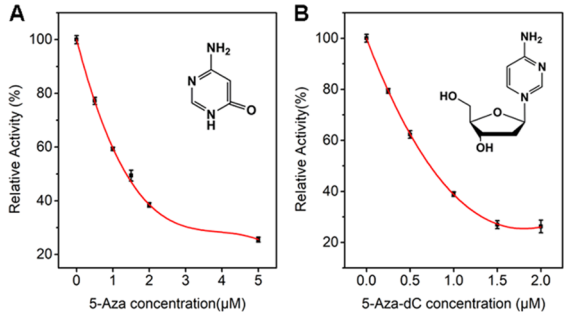

Figure 6. Variance of the M.SssI MTase relative activity induced by different concentrations of (A) 5-Aza and (B) 5-Aza-dc. The 100 U mL^{-1} M.SssI MTase was used in the experiments. Error bars represent the standard deviation of three experiments.

https://dx.doi.org/10.1021/acs.analchem.0c04904
Anal. Chem. 2021, 93, 2974−2981

2.7. Selectivity, Stability, and Reproducibility of the ECL Biosensor. The selectivity of the ECL biosensor was investigated by introducing different interference enzymes including DNA adenine MTase (Dam) and HhaI MTase. Dam MTase can methylate the adenine residues in the sequence 5′-GATC-3′,[66] and HhaI MTase can catalyze the methylation of cytosine residues in the sequence 5′-GCGC-3′.[67] As shown in Figure 7A, an extremely small chemiluminescence signal is observed in response to either Dam MTase (Figure 7, red column) or HhaI MTase (Figure 7, green column), while a high ECL signal is observed in response to M.SssI MTase (Figure 7, blue column). This can be explained by the fact that neither HhaI nor Dam MTase can methylate the CpG dinucleotide site in the sequence 5′-CCGG-3′. These results indicate the excellent selectivity of the proposed biosensor toward M.SssI. The stability of the ECL biosensor was investigated by measuring 100 U mL^{-1} M.SssI MTase under 15 consecutive cycle scans. Stable and continuous ECL signals with a relative standard deviation (RSD) of 1.40% are observed even after 15 cycle scans (Figure 7B). The reproducibility of the ECL biosensor was studied by measuring 100 U mL^{-1} M.SssI MTase with three electrodes fabricated under identical conditions. The measured RSD is 0.39%, indicating the good reproducibility of this biosensor for M.SssI MTase assay.

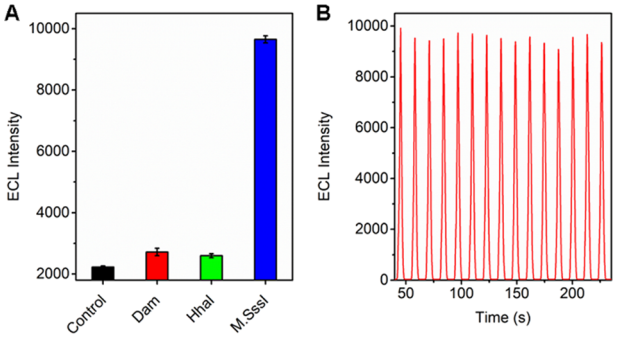

Figure 7. (A) ECL intensity induced by 100 U mL^{-1} HhaI MTase, 100 U mL^{-1} M.SssI MTase, and 100 U mL^{-1} Dam MTase. Error bars represent the standard deviation of three experiments. (B) Stability assessment of the ECL biosensor by continuous scanning for 15 cycles.

3.8. Measurement of M.SssI MTase Activity in Serum Samples. To demonstrate the proof-of-concept of complex biological samples analysis, we spiked M.SssI MTase into human serum to perform the recovery experiments. The obtained recovery is in a range of 97.9−119.0% with an RSD of 3.1−4.9% (Table S2). These results suggest the potential applications of this ECL biosensor in biomedical research.

3. CONCLUSIONS

We have demonstrated for the first time the development of a host−guest interaction-based and MOG-based biosensor with aggregation-induced ECL enhancement for M.SssI MTase assay. This biosensor employs a MOG as the luminophor and potassium persulfate as the coreactant, and the formation of the Ag-MOG from the aggregation of silver nanoclusters can induce significant ECL enhancement. The proposed ECL biosensor has significant advantages: (1) the synthesis of the Ag-MOG is very facile; (2) the significant ECL signal enhancement results from the aggregation of Ag_9NCs; (3) the supramolecular guest−host recognition enables easy capturing of redox molecules (Fc) for efficiently quenching the ECL signal of the Ag-MOG; (4) the ECL biosensor enables one-step detection of M.SssI MTase; and (5) the ECL biosensor exhibits good specificity, high sensitivity, excellent stability, and reproducibility. This biosensor can accurately measure M.SssI MTase in human serum and screen the potential inhibitors as well. Moreover, this biosensor can be easily extended to detect other DNA methyltransferases and DNA-modifying enzymes by simply changing the recognition sequence, with potential applications in biomedical research and disease diagnosis.

■ ASSOCIATED CONTENT

Supporting Information

The Supporting Information is available free of charge at https://pubs.acs.org/doi/10.1021/acs.analchem.0c04904.

Characterization of the Ag-MOG, ECL property of the Ag_9NCs- and H_2mba-modified GCE, optimization of experimental conditions, comparison of the proposed ECL biosensor with the reported methods for M.SssI MTase assay, and real sample analysis (PDF)

■ AUTHOR INFORMATION

Corresponding Authors

Xiliang Luo − *Key Laboratory of Optic-electric Sensing and Analytical Chemistry for Life Science, MOE; Shandong Key Laboratory of Biochemical Analysis; Key Laboratory of Analytical Chemistry for Life Science in Universities of Shandong; and College of Chemistry and Molecular Engineering, Qingdao University of Science and Technology, Qingdao 266042, P. R. China;* orcid.org/0000-0001-6075-7089; Email: xiliangluo@qust.edu.cn

Chun-yang Zhang − *College of Chemistry, Chemical Engineering and Materials Science, Collaborative Innovation Center of Functionalized Probes for Chemical Imaging in Universities of Shandong, Key Laboratory of Molecular and Nano Probes, Ministry of Education, Shandong Provincial Key Laboratory of Clean Production of Fine Chemicals, Shandong Normal University, Jinan 250014, China;* orcid.org/0000-0002-8010-1981; Phone: +86 0531-86186033; Email: cyzhang@sdnu.edu.cn; Fax: +86 0531-82615258

Authors

Lin Cui − *College of Chemistry, Chemical Engineering and Materials Science, Collaborative Innovation Center of Functionalized Probes for Chemical Imaging in Universities of Shandong, Key Laboratory of Molecular and Nano Probes, Ministry of Education, Shandong Provincial Key Laboratory of Clean Production of Fine Chemicals, Shandong Normal University, Jinan 250014, China*

Min-hui Zhao − *College of Chemistry, Chemical Engineering and Materials Science, Collaborative Innovation Center of Functionalized Probes for Chemical Imaging in Universities of Shandong, Key Laboratory of Molecular and Nano Probes, Ministry of Education, Shandong Provincial Key Laboratory of Clean Production of Fine Chemicals, Shandong Normal University, Jinan 250014, China*

Chen-chen Li − *College of Chemistry, Chemical Engineering and Materials Science, Collaborative Innovation Center of Functionalized Probes for Chemical Imaging in Universities of Shandong, Key Laboratory of Molecular and Nano Probes,*

https://dx.doi.org/10.1021/acs.analchem.0c04904
Anal. Chem. 2021, 93, 2974−2981

Ministry of Education, Shandong Provincial Key Laboratory of Clean Production of Fine Chemicals, Shandong Normal University, Jinan 250014, China; Key Laboratory of Optic-electric Sensing and Analytical Chemistry for Life Science, MOE; Shandong Key Laboratory of Biochemical Analysis; Key Laboratory of Analytical Chemistry for Life Science in Universities of Shandong; and College of Chemistry and Molecular Engineering, Qingdao University of Science and Technology, Qingdao 266042, P. R. China

Quanbo Wang − *Laboratory of Immunology for Environment and Health, Shandong Analysis and Test Center, Qilu University of Technology (Shandong Academy of Sciences), Jinan, Shandong 250014, China*

Complete contact information is available at: https://pubs.acs.org/10.1021/acs.analchem.0c04904

Author Contributions

[†]L.C., M.Z., and C.L. contributed equally.

Notes

The authors declare no competing financial interest.

■ ACKNOWLEDGMENTS

This work was supported by the National Natural Science Foundation of China (grant nos. 21735003, 21605096, and 21974080), the Taishan Scholar Program of Shandong Province of China (ts20110829), and the Award for Team Leader Program of Taishan Scholars of Shandong Province, China.

■ REFERENCES

(1) Jurkowska, R. Z.; Jurkowski, T. P.; Jeltsch, A. *ChemBioChem* **2011**, *12*, 206−222.
(2) Li, E.; Beard, C.; Jaenisch, R. *Nature* **1993**, *366*, 362−365.
(3) Shukla, V.; Coumoul, X.; Lahusen, T.; Wang, R. H.; Xu, X.; Vassilopoulos, A.; Xiao, C.; Lee, M.-H.; Man, Y.-G.; Ouchi, M.; Ouchi, T.; Deng, C.-X. *Cell Res.* **2010**, *20*, 1201−1215.
(4) Wu, P.; Cai, J.; Chen, Q.; Han, B.; Meng, X.; Li, Y.; Li, Z.; Wang, R.; Lin, L.; Duan, C.; Kang, C.; Jiang, C. *Nat. Commun.* **2019**, *10*, 2045.
(5) Lopez Torres, A.; Yanez Barrientos, E.; Wrobel, K.; Wrobel, K. *Anal. Chem.* **2011**, *83*, 7999−8005.
(6) Ogino, S.; Kawasaki, T.; Brahmandam, M.; Cantor, M.; Kirkner, G. J.; Spiegelman, D.; Makrigiorgos, G. M.; Weisenberger, D. J.; Laird, P. W.; Loda, M.; Fuchs, C. S. *J. Mol. Diagn.* **2006**, *8*, 209−217.
(7) Singer, J.; Schnute, W. C., Jr.; Shively, J. E.; Todd, C. W.; Riggs, A. D. *Anal. Biochem.* **1979**, *94*, 297−301.
(8) Su, F.; Wang, L.; Sun, Y.; Liu, C.; Duan, X.; Li, Z. *Chem. Sci.* **2015**, *6*, 1866−1872.
(9) Song, G.; Chen, C.; Ren, J.; Qu, X. *ACS Nano* **2009**, *3*, 1183−1189.
(10) Zhang, H.; Zhang, K.; Yao, Y.; Liu, Y.; Ji, J.; Huang, X.; Liu, J.; Liu, B. *Anal. Chem.* **2019**, *91*, 9500−9507.
(11) Zhou, X.; Zhao, M.; Duan, X.; Guo, B.; Cheng, W.; Ding, S.; Ju, H. *ACS Appl. Mater. Interfaces* **2017**, *9*, 40087−40093.
(12) Li, X.; Meng, M.; Zheng, L.; Xu, Z.; Song, P.; Yin, Y.; Eremin, S. A.; Xi, R. *Anal. Chem.* **2016**, *88*, 8556−8561.
(13) Wang, Z. Y.; Li, P.; Cui, L.; Xu, Q.; Zhang, C. Y. *Anal. Chem.* **2020**, *92*, 13573−13580.
(14) Richter, M. M. *Chem. Rev.* **2004**, *104*, 3003−3036.
(15) Cui, L.; Yu, S.; Gao, W.; Zhang, X.; Deng, S.; Zhang, C. Y. *ACS Appl. Mater. Interfaces* **2020**, *12*, 7966−7973.
(16) Liu, Z.; Qi, W.; Xu, G. *Chem. Soc. Rev.* **2015**, *44*, 3117−3142.
(17) Liu, Y.; Lei, J.; Huang, Y.; Ju, H. *Anal. Chem.* **2014**, *86*, 8735−8741.
(18) Zhao, M. H.; Cui, L.; Zhang, C. Y. *Chem. Commun.* **2020**, *56*, 2971−2974.
(19) Fang, Y.; Wang, H. M.; Gu, Y. X.; Yu, L.; Wang, A. J.; Yuan, P. X.; Feng, J. J. *Anal. Chem.* **2020**, *92*, 3206−3212.
(20) Jiang, W.; Wu, L.; Duan, J.; Yin, H.; Ai, S. *Biosens. Bioelectron.* **2018**, *99*, 660−666.
(21) Zhou, Y.; Chen, S.; Luo, X.; Chai, Y.; Yuan, R. *Anal. Chem.* **2018**, *90*, 10024−10030.
(22) Liu, X.; Jiang, H.; Lei, J.; Ju, H. *Anal. Chem.* **2007**, *79*, 8055−8060.
(23) Tan, X.; Zhang, B.; Zou, G. *J. Am. Chem. Soc.* **2017**, *139*, 8772−8776.
(24) Zhou, Z.; Xie, S.; Chen, X.; Tu, Y.; Xiang, J.; Wang, J.; He, Z.; Zeng, Z.; Tang, B. Z. *J. Am. Chem. Soc.* **2019**, *141*, 9803−9807.
(25) Sanji, T.; Nakamura, M.; Kawamata, S.; Tanaka, M.; Itagaki, S.; Gunji, T. *Chem. − Eur. J.* **2012**, *18*, 15254−15257.
(26) Han, Z.; Zhang, Y.; Wu, Y.; Li, Z.; Bai, L.; Huo, S.; Lu, X. *Anal. Chem.* **2019**, *91*, 8676−8682.
(27) Kwok, R. T. K.; Leung, C. W. T.; Lam, J. W. Y.; Tang, B. Z. *Chem. Soc. Rev.* **2015**, *44*, 4228−4238.
(28) Wu, W.; Feng, G.; Xu, S.; Liu, B. *Macromolecules* **2016**, *49*, 5017−5025.
(29) Mei, J.; Hong, Y.; Lam, J. W.; Qin, A.; Tang, Y.; Tang, B. Z. *Adv. Mater.* **2014**, *26*, 5429−5479.
(30) Luo, Z.; Yuan, X.; Yu, Y.; Zhang, Q.; Leong, D. T.; Lee, J. Y.; Xie, J. *J. Am. Chem. Soc.* **2012**, *134*, 16662−16670.
(31) Zhang, L.; Zhu, J.; Zhou, Z.; Guo, S.; Li, J.; Dong, S.; Wang, E. *Chem. Sci.* **2013**, *4*, 4004−4010.
(32) Karimi, M.; Sahandi Zangabad, P.; Baghaee-Ravari, S.; Ghazadeh, M.; Mirshekari, H.; Hamblin, M. R. *J. Am. Chem. Soc.* **2017**, *139*, 4584−4610.
(33) Chen, C.; Li, R. H.; Zhu, B. S.; Wang, K. H.; Yao, J. S.; Yin, Y. C.; Yao, M. M.; Yao, H. B.; Yu, S. H. *Am. Ethnol.* **2018**, *130*, 7224−7228.
(34) Yin, M.-M.; Chen, W.-Q.; Liu, Y.; Jiang, F.-L. *ACS Appl. Nano Mater.* **2019**, *2*, 408−417.
(35) Sugiuchi, M.; Maeba, J.; Okubo, N.; Iwamura, M.; Nozaki, K.; Konishi, K. *J. Am. Chem. Soc.* **2017**, *139*, 17731−17734.
(36) Carrara, S.; Aliprandi, A.; Hogan, C. F.; De Cola, L. *J. Am. Chem. Soc.* **2017**, *139*, 14605−14610.
(37) Wei, X.; Zhu, M.-J.; Cheng, Z.; Lee, M.; Yan, H.; Lu, C.; Xu, J.-J. *Angew. Chem., Int. Ed.* **2019**, *58*, 3162−3166.
(38) Liu, J. L.; Zhang, J. Q.; Tang, Z. L.; Zhuo, Y.; Chai, Y. Q.; Yuan, R. *Chem. Sci.* **2019**, *10*, 4497−4501.
(39) Wu, Q.; He, L.; Jiang, Z. W.; Li, Y.; Zhao, T. T.; Li, Y. H.; Huang, C. Z.; Li, Y. F. *J. Environ. Sci.* **2019**, *86*, 203−212.
(40) He, L.; Jiang, Z. W.; Li, W.; Li, C. M.; Huang, C. Z.; Li, Y. F. *ACS Appl. Mater. Interfaces* **2018**, *10*, 28868−28876.
(41) Piepenbrock, M. O. M.; Lloyd, G. O.; Clarke, N.; Steed, J. W. *Chem. Rev.* **2010**, *110*, 1960−2004.
(42) Zhang, J.; Su, C. Y. *Coord. Chem. Rev.* **2013**, *257*, 1373−1408.
(43) He, L.; Peng, Z. W.; Jiang, Z. W.; Tang, X. Q.; Huang, C. Z.; Li, Y. F. *ACS Appl. Mater. Interfaces* **2017**, *9*, 31834−31840.
(44) He, L.; Li, Y.; Wu, Q.; Wang, D. M.; Li, C. M.; Huang, C. Z.; Li, Y. F. *ACS Appl. Mater. Interfaces* **2019**, *11*, 29158−29166.
(45) Li, X.; Li, J.; Gao, Y.; Kuang, Y.; Shi, J.; Xu, B. *J. Am. Chem. Soc.* **2010**, *132*, 17707−17709.
(46) Li, Y.; Guo, M. X.; He, L.; Huang, C. Z.; Li, Y. F. *ACS Sustainable Chem. Eng.* **2019**, *7*, 5292−5299.
(47) Li, Y.; Huang, C. Z.; Li, Y. F. *Anal. Chem.* **2019**, *91*, 9308−9314.
(48) Li, Y.; He, L.; Huang, C. Z.; Li, Y. F. *Biosens. Bioelectron.* **2019**, *134*, 29−35.
(49) Li, Y.; Jiang, Z. W.; Xiao, S. Y.; Huang, C. Z.; Li, Y. F. *Anal. Chem.* **2018**, *90*, 12191−12197.
(50) Roy, S.; Katiyar, A. K.; Mondal, S. P.; Ray, S. K.; Biradha, K. *ACS Appl. Mater. Interfaces* **2014**, *6*, 11493−11501.
(51) Sun, Y.; Giebink, N. C.; Kanno, H.; Ma, B.; Thompson, M. E.; Forrest, S. R. *Nature* **2006**, *440*, 908−912.

(52) Sui, J.; Wang, L.; Zhao, W.; Hao, J. *Chem. Commun.* **2016**, *52*, 6993−6996.
(53) Jayaramulu, K.; Geyer, F.; Petr, M.; Zboril, R.; Vollmer, D.; Fischer, R. A. *Adv. Mater.* **2017**, *29*, 1605307.
(54) Xie, Z.; Sun, P.; Wang, Z.; Li, H.; Yu, L.; Sun, D.; Chen, M.; Bi, Y.; Xin, X.; Hao, J. *Angew. Chem.* **2020**, *132*, 10008−10013.
(55) Luo, X.; Li, Y.; Zheng, J.; Qi, H.; Liang, Z.; Ning, X. *Chem. Commun.* **2015**, *51*, 9487−9490.
(56) Zhang, H.; Yang, Y.; Dong, H.; Cai, C. *Biosens. Bioelectron.* **2016**, *86*, 927−932.
(57) Gao, F.; Fan, T.; Ou, S.; Wu, J.; Zhang, X.; Luo, J.; Li, N.; Yao, Y.; Mou, Y.; Liao, X.; Geng, D. *Biosens. Bioelectron.* **2018**, *99*, 201−208.
(58) Yin, H.; Zhou, Y.; Xu, Z.; Chen, L.; Zhang, D.; Ai, S. *Biosens. Bioelectron.* **2013**, *41*, 492−497.
(59) Li, W.; Wu, P.; Zhang, H.; Cai, C. *Anal. Chem.* **2012**, *84*, 7583−7590.
(60) Wang, G. L.; Zhou, L. Y.; Luo, H. Q.; Li, N. B. *Anal. Chim. Acta* **2013**, *768*, 76−81.
(61) Yang, Z.; Wang, F.; Wang, M.; Yin, H.; Ai, S. *Biosens. Bioelectron.* **2015**, *66*, 109−114.
(62) Karimi, M. A.; Dadmehr, M.; Hosseini, M.; Korouzhdehi, B.; Oroojalian, F. *RSC Adv.* **2019**, *9*, 12063−12069.
(63) Liu, P.; Yang, X. H.; Wang, Q.; Huang, J.; Liu, J. B.; Zhu, Y.; He, L. L.; Wang, K. M. *Chin. Chem. Lett.* **2014**, *25*, 1047−1051.
(64) Li, Z. M.; Zhong, Z. H.; Liang, R. P.; Qiu, J. D. *Sens. Actuators B Chem.* **2017**, *238*, 626−632.
(65) Xia, Y.; Wu, L.; Hu, Y.; He, Y.; Cao, Z.; Zhu, X.; Yi, X.; Wang, J. *Biosens. Bioelectron.* **2019**, *126*, 269−274.
(66) Horton, J. R.; Liebert, K.; Bekes, M.; Jeltsch, A.; Cheng, X. *J. Mol. Biol.* **2006**, *358*, 559−570.
(67) Wu, J. C.; Santi, D. V. *J. Biol. Chem.* **1987**, *262*, 4778−4786.

https://dx.doi.org/10.1021/acs.analchem.0c04904
Anal. Chem. 2021, 93, 2974−2981